JACS
JOURNAL OF THE AMERICAN CHEMICAL SOCIETY
Article
pubs.acs.org/JACS

Studying "Invisible" Excited Protein States in Slow Exchange with a Major State Conformation

Pramodh Vallurupalli,*[,†,§] Guillaume Bouvignies,[†,§] and Lewis E. Kay*[,†,‡]

[†]Departments of Molecular Genetics, Biochemistry, and Chemistry, The University of Toronto, Toronto, Ontario, Canada M5S 1A8
[‡]Program in Molecular Structure and Function, Hospital for Sick Children, 555 University Avenue, Toronto, Ontario, Canada M5G 1X8

Supporting Information

ABSTRACT: Ever since its initial development, solution NMR spectroscopy has been used as a tool to study conformational exchange. Although many systems are amenable to relaxation dispersion approaches, cases involving highly skewed populations in slow chemical exchange have, in general, remained recalcitrant to study. Here an experiment to detect and characterize "invisible" excited protein states in slow exchange with a visible ground-state conformation (excited-state lifetimes ranging from ∼5 to 50 ms) is presented. This method, which is an adaptation of the chemical exchange saturation transfer (CEST) magnetic resonance imaging experiment, involves irradiating various regions of the spectrum with a weak B_1 field while monitoring the effect on the visible major-state peaks. The variation in major-state peak intensities as a function of frequency offset and B_1 field strength is quantified to obtain the minor-state population, its lifetime, and excited-state chemical shifts and line widths. The methodology was validated with ^{15}N CEST experiments recorded on an SH3 domain−ligand exchanging system and subsequently used to study the folding transition of the A39G FF domain, where the invisible unfolded state has a lifetime of ∼20 ms. Far more accurate exchange parameters and chemical shifts were obtained than via analysis of Carr−Purcell−Meiboom−Gill relaxation dispersion data.

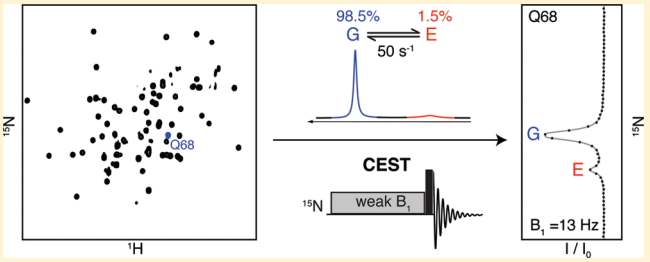

INTRODUCTION

Proteins are dynamic molecules that are best described in terms of ensembles of interconverting conformations.[1,2] The lifetimes of the exchanging conformers, their populations, and indeed their functions can vary significantly within the ensemble.[1−4] A quantitative understanding of this important class of biomolecule is therefore predicated on a detailed characterization of the kinetics and thermodynamics of the exchange process(es)[2,5,6] and on the determination of atomic-resolution structures of the many different conformers that populate the proteins' energy landscape.[7−11] This is, in general, difficult to accomplish. Standard methods of structural biology are most successful when applied to a "pure" sample consisting of only a single highly populated conformation. Conformers that are transiently formed and populated at only very low levels, designated in what follows as "invisible" or excited conformational states (excited states for short), have remained recalcitrant to detailed quantitative analysis. This situation is changing, however, with the development of new biophysical approaches, including solution-based NMR methods that "study" exchange processes by monitoring the positions[12] and line widths of peaks derived from the "visible" ground state.[13−15] Of particular note is the so-called Carr−Purcell−Meiboom−Gill (CPMG) relaxation dispersion experiment,[16,17] in which a series of refocusing pulses are applied to the evolving transverse magnetization, leading to a modulation of the chemical shift difference between nuclei in the different exchanging states, $|\Delta\tilde{\omega}|$ (in ppm), and hence of the effective transverse relaxation of the observed major-state spins.[13,14] This modulation can be "fit" to extract the kinetics and thermodynamics of the exchange process as well as the $|\Delta\tilde{\omega}|$ values for each exchanging spin[18] so long as the rates of exchange lie between ∼200 and 2000 s^{-1} and the fractional population of the excited state is in excess of 0.5%. Over the past decade, CPMG experiments have been extended to studies of protein chemical exchange, from which it has become possible to extract excited-state ^{1}H, ^{13}C, and ^{15}N backbone chemical shifts[19−23] and many of the side-chain chemical shifts[24−27] along with the orientations of bond vectors.[28,29] Recently, data of this sort has been used to produce atomic-resolution models of excited states for a number of different exchanging systems.[10,11,30]

A significant limitation of the CPMG experiment is the relatively small exchange time scale window over which the interconversion process can be quantified (see above). To address this, we recently introduced an approach whereby CPMG relaxation dispersion profiles are fit in concert with major-state peak shifts in HSQC/HMQC spectra[31] that extends the CPMG method to include systems with exchange

Received: January 5, 2012
Published: May 3, 2012

   dx.doi.org/10.1021/ja3001419 | J. Am. Chem. Soc. 2012, 134, 8148−8161

rates as high as 6000 s^{-1}. At the opposite end of the exchange spectrum, systems with interconversion rates less than ~100 s^{-1} can be studied using magnetization-exchange-based experiments so long as the interconverting states can be observed in spectra.[14,32] Cases where the populations are highly skewed (so only peaks from the ground-state conformer are obtained) and the exchange is slow have remained enigmatic, however, because they are not in general amenable to study using either CPMG or typical exchange-type experiments of the sort involving exchange of unperturbed longitudinal magnetization. It is the study of exchanging systems in this regime that we address here.

Like the CPMG method, which was developed over 50 years ago[16,17] and has subsequently found applications in biomolecular NMR spectroscopy,[21,33] the "saturation transfer" class of experiments was originated in the early 1960s by Forsen and Hoffman.[34] In these experiments, a weak field is applied at the position of an exchanging peak of interest, and the "perturbation" that results (not necessarily saturation) is transferred to the interconverting state via chemical exchange.[35−39] Gupta and Redfield[40] applied this approach to study electron exchange between ferri- and ferrocytochrome *c* in a sample with approximately equal concentrations of reduced and oxidized protein and to assign methyl resonances in the ferro state by saturation transfer from the corresponding well-resolved, hyperfine-shifted peaks of the ferri conformer. Feeney and Roberts used this methodology to assign the chemical shifts of small molecules such as cofactors and inhibitors bound to enzymes. In one such study involving dihydrofolate reductase, ^{1}H saturation from 2 to 7 ppm in small steps allowed the identification of the small-molecule bound-state peak positions by perturbations to peaks derived from the well-resolved free state.[41] Later on, Balaban and colleagues[37] and subsequently van Zijl and Yadav[42] developed one-dimensional chemical exchange saturation transfer (CEST) spectroscopy, by which very low amplitude invisible signals from metabolites and proteins can be amplified manyfold and "read out" from the water resonance so long as the nuclei of interest exchange with water. Clore, Torchia, and co-workers introduced an elegant two-dimensional (2D) experiment, dark-state exchange saturation transfer (DEST), to determine both the kinetics of interconversion between free amyloid-β (Aβ) peptide and very high molecular weight Aβ protofibrils and the ^{15}N line widths of the invisible ("dark")-state resonances.[35] Building on the DEST experiment, we show here that CEST-type experiments can be used to quantify slow chemical exchange precisely in the regime that challenges the CPMG approach, providing the kinetics and thermodynamics of the exchange process as well as the chemical shifts of the excited-state nuclei often from direct inspection of the resulting spectra. The methodology was cross-validated with a protein−ligand two-state exchanging system that has been studied previously,[28] with an exchange rate and minor state population of ~150 s^{-1} and 2.5% (5 °C), respectively. Subsequently, the utility of the experiment was demonstrated with an application to the folding of the A39G FF domain,[11,43] for which the CPMG dispersion profiles are very small and hence difficult to analyze. Accurate exchange parameters (51.6 ± 1 s^{-1} and 1.65 ± 0.02%) as well as excited-state chemical shifts were obtained via the CEST methodology. In contrast to other methods for studying invisible states (CPMG or $R_{1\rho}$ relaxation dispersion, D-evolution), robust exchange parameters were obtained from fits of data recorded on a per-residue basis measured at a single magnetic field strength, allowing a rigorous evaluation of the two-state assumption that is often used in fits of dispersion data.

RESULTS AND DISCUSSION

Comparison of CPMG and CEST for Studies of Chemical Exchange. Prior to a discussion of experimental details and applications to exchanging systems, we provide a brief discussion of the basic features of the CEST experiment and present an analogy with the CPMG methodology that illustrates some of the similarities between the two approaches. For simplicity, in what follows we consider an isolated ^{15}N spin in a protein exchanging between two conformations, G (ground) and E (excited),

$$\mathrm{G} \underset{k_{EG}}{\overset{k_{GE}}{\rightleftarrows}} \mathrm{E}$$

with distinct chemical shifts $\tilde{\omega}_G$ and $\tilde{\omega}_E$ ($\Delta\tilde{\omega} = \tilde{\omega}_E - \tilde{\omega}_G$) in each of the two states (Figure 1A). The fractional populations of states G and E, $p_G \gg p_E$, are given by $p_G = k_{EG}/k_{ex}$ and $p_E = k_{GE}/k_{ex} = 1 - p_G$, where $k_{ex} = k_{GE} + k_{EG}$. In the cases of interest here, only major-state peaks are visible in the spectra, although in Figure 1A the excited-state correlation (red) is also shown for clarity. To simplify the discussion, we will assume that chemical exchange occurs in the slow-exchange limit, where $k_{ex} \ll \Delta\omega$ (i.e., we do not consider multiple transfers of magnetization between the states).

Figure 1B illustrates the basic CPMG pulse train that is used to study exchanging systems in the approximate regime 200 $s^{-1} \le k_{ex} \le 2000$ s^{-1} and $p_E \ge 0.5\%$. Here the effective transverse relaxation rates ($R_{2,eff}$) of the visible peaks are quantified as a function of the frequency $\nu_{CPMG} = 1/(4\tau_{CPMG})$ at which refocusing 180° pulses are applied during a relaxation delay T_{relax}. The evolution of magnetization is illustrated in Figure 1C, where without any loss in generality it has been assumed that the carrier is placed on resonance for the major-state correlation being considered (i.e., at $\tilde{\omega}_G$). After the 90° pulse at the start of the echo train, magnetization from this state remains aligned along the *y* axis in the rotating frame while the magnetization from the minor state precesses in the *xy* plane, losing phase with the ground state. On average, the excited-state spins accumulate a phase of $\langle\phi\rangle = \Delta\omega/k_{EG}$ between exchange events, so exchange leads to a reduction in the major-state signal and hence a nonzero exchange-induced relaxation rate R_{ex}. Each 180° pulse of the CPMG train inverts the sense in which the spins precess around the *z* axis, reducing the phase accumulation $\langle\phi\rangle$ and decreasing R_{ex}. Exchange parameters and minor-state chemical shifts can be obtained from fits of the $R_{2,eff}(\nu_{CPMG})$ profile so long as the exchange contribution to $R_{2,eff}$ (i.e., R_{ex}) is quenched as ν_{CPMG} increases (Figure 1D). In the slow-exchange limit, $R_{ex} = k_{GE}$ when $\nu_{CPMG} = 0$, so the maximum observable change in the $R_{2,eff}(\nu_{CPMG})$ profile is k_{GE}.

By means of example, consider an exchanging system in the window of interest here with $k_{ex} = 50$ s^{-1} and $p_E = 1.5\%$, for which $k_{GE} = 0.75$ s^{-1}. If a contribution of 10 s^{-1} to $R_{2,eff}$ from intrinsic relaxation is assumed, the maximum loss in the detected signal intensity during a "typical" T_{relax} delay of 50 ms from chemical exchange, which occurs when $\nu_{CPMG} \to 0$, is $1 - e^{-(10.75)(0.05)}/e^{-(10)(0.05)} \approx 3.7\%$. Quantifying such a small change accurately in the presence of noise and systematic errors is very difficult, compromising the accuracy of the exchange parameters obtained from CPMG relaxation dispersion data in this limit.

dx.doi.org/10.1021/ja3001419 | J. Am. Chem. Soc. 2012, 134, 8148−8161

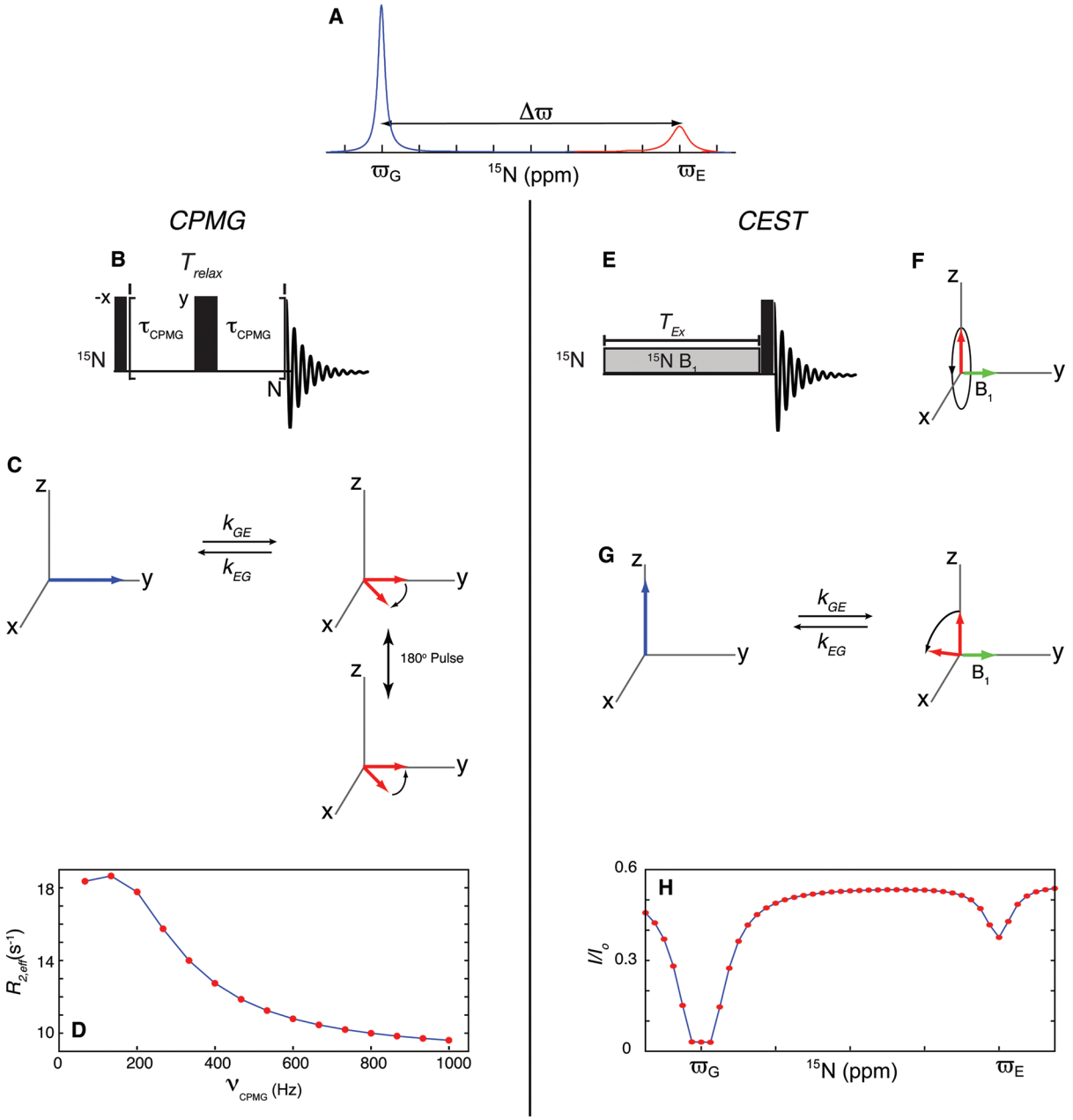

Figure 1. Comparison of the standard CPMG experiment with the weak B_1 CEST experiment proposed here. (A) ^{15}N spectrum of an isolated spin exchanging between two states with chemical shifts $\tilde{\omega}_G$ and $\tilde{\omega}_E$. The minor state is shown in the spectrum for purposes of illustration but cannot be observed in the systems of interest. (B) Basic CPMG experiment, with narrow and wide pulses denoting 90° and 180° flip angles, respectively. A variable number (N) of 180° refocusing pulses is applied during a constant-time relaxation element of duration T_{relax}. (C) Illustration of the mechanism underlying the CPMG experiment, with the major-state peak (blue) assumed to be on resonance. The 180° pulses invert the sense in which "excited-state" spins (red magnetization) precess around the external magnetic field (B_0). Stochastic modulation of the chemical shifts of the interconverting spins leads to a dephasing of the magnetization. (D) Typical relaxation dispersion curve obtained by quantifying the peak intensities in a CPMG experiment. (E) Schematic of the CEST experiment. A weak B_1 field is applied along the y axis (green) for a time T_{EX} before acquisition of the spectrum. (F) When the B_1 field is on resonance with the minor state, precession occurs around the y axis, in analogy to what is shown in (C) for the CPMG experiment. (G) Precession leads to a phase accumulation with respect to the magnetization in the major state and a subsequent reduction in the magnetization intensity of the major state from the constant exchange between states. (H) Intensity profile obtained by quantifying the intensity of the visible-state peak as a function of position of the weak B_1 irradiation field. The ratio I/I_0 is plotted, where I is the intensity after an irradiation period of duration T_{EX} and I_0 is the intensity when $T_{EX} = 0$. There is a loss of intensity when the weak continuous-wave field is resonant with the major and minor states.

The situation changes, however, when the value of T_{relax} can be increased significantly, allowing a larger number of exchange events to occur. This can be accomplished by doing experiments that exploit coherences with smaller intrinsic relaxation rates.[44−46] For example, when the intrinsic relaxation rate is 1 s^{-1} and T_{relax} = 500 ms, the fractional loss of signal due to exchange becomes $1 - e^{-(1.75)(0.5)}/e^{-(1)(0.5)} \approx 31\%$, an amount that can easily be quantified. One approach is to use a longitudinal-magnetization-based experiment, since in protein applications the longitudinal relaxation rates (R_1) can be an

dx.doi.org/10.1021/ja3001419 | J. Am. Chem. Soc. 2012, 134, 8148−8161

order of magnitude or more lower than the transverse relaxation rates R_2. For this reason, CEST-based experiments offer an attractive avenue for the study of slowly exchanging systems.

The CEST experiment is illustrated schematically in Figure 1E; in what follows, we initially assume that $R_1 = R_2 = 0$ (but see below). A weak B_1 field (ν_1 = 5−50 Hz for the studies described here) is applied at a specific offset from the major-state peak for a time T_{EX}, followed by a 90° pulse and recording of the ^{15}N spectrum. Successive experiments "step" the weak field through the entire spectrum, and the intensity of the visible major-state peak is quantified as a function of offset to detect the position of the corresponding minor-state correlation. When the B_1 offset is far from either the major- or minor-state correlation, it has no effect on the spins of interest, and the intensity of the major-state peak is unaffected relative to the case where $B_1 = 0$. However, when the field is placed at $\tilde{\omega}_E$ (green vector in Figure 1F), it induces Rabi oscillations in the nuclei transiently populating the minor state, leading to precession around the y axis in the xz plane in analogy to the precession about the z axis that occurs in a CPMG experiment (Figure 1C). The bulk magnetization vector corresponding to the excited state rotates on average by an angle $\langle\theta\rangle = 2\pi\nu_1/k_{EG}$ around the y axis between exchange events (Figure 1G), leading to a net reduction in the polarization of the ground state that is detected, leading to the profile illustrated in Figure 1H. Here the intensity I of the major-state correlation (normalized to I_0, the intensity when $T_{EX} = 0$) is plotted as a function of the position of the B_1 field. The reduction in the observed magnetization of state G when the B_1 field overlaps with the minor-state peak is clearly seen. This phenomenon is directly analogous to chemical-exchange-induced line broadening, with ν_1 in CEST corresponding to $\Delta\omega/2\pi$ ($\Delta\omega = \omega_E - \omega_G$) in the CPMG experiment. Therefore, in direct analogy with CPMG relaxation dispersion, the intensity of the major-state correlation as a function of T_{EX} in the $p_G \gg p_E$ limit can be calculated from the following approximate expression for R_{ex} derived by Millet et al.:[47]

$$I(T_{EX}) = I_0 \exp(-R_{ex}T_{EX}) \tag{1}$$

where

$$R_{ex} = \frac{p_G p_E k_{ex}}{1 + \left(\frac{k_{ex}}{2\pi\nu_1}\right)^2}$$

The above discussion assumed that that $R_1 = R_2 = 0$. In general, the situation is more complicated because relaxation occurs during precession of the magnetization about B_1 and potentially also saturation. If exchange is neglected, the time dependence of the z component of the magnetization upon application of an on-resonance B_1 field is given by

$$M_z(T_{EX}) = M_0\left(\frac{R_1R_2}{\omega_1^2 + R_1R_2} + f(T_{EX})\frac{\omega_1^2}{\omega_1^2 + R_1R_2}\right) \tag{2.1}$$

where

$$f(T_{EX}) = \begin{cases} [\cos(\rho T_{EX}) + R_{avg}T_{EX}\,\mathrm{sinc}(\rho T_{EX})] & |\omega_1| \geq \Delta R \\ \quad \times \exp(-R_{avg}T_{EX}), & \\ [\cosh(\rho T_{EX}) + R_{avg}T_{EX}\,\mathrm{sinhc}(\rho T_{EX})] & |\omega_1| < \Delta R \\ \quad \times \exp(-R_{avg}T_{EX}), & \end{cases} \tag{2.2}$$

and $R_{avg} = (R_1 + R_2)/2$, $\Delta R = (R_2 - R_1)/2$, $\rho = |\omega_1^2 - (\Delta R)^2|^{1/2}$, and $\omega_1 = \gamma B_1$. From eqs 2.1 and 2.2, it can be seen that magnetization decays to the steady-state value $M_0R_1R_2/(\omega_1^2 + R_1R_2)$ with a time constant R_{avg}. The corresponding solution of the Bloch equations that includes chemical exchange and a weak B_1 field corresponding to the CEST experiment is complicated and offers little understanding in its most general form.[48,49] However, some insight can be obtained from the expressions that neglect exchange (eqs 2.1 and 2.2). For example, if the lifetime of the excited state, $1/k_{EG}$, is such that $1/k_{EG} \leq T_{EX}$ and $R_{avg}/k_{EG} > 1$, then the excited-state magnetization approaches its steady-state value [i.e., $f(T_{EX}) \approx 0$ in eq 2.1 since $\exp(-R_{avg}/k_{EG})$ is small], which is close to zero (saturation) even for small values of ω_1 and typical relaxation rates (e.g., $\omega_1 = 2\pi \times 10$ rad/s, $R_1 \approx 1$ s^{-1}, R_2 = 5−20 s^{-1}). In this case, chemical exchange transfers the saturation from state E to G, with the magnetization in the E state subsequently "replenished" by exchange from G to E, leading to a decrease in the magnetization of the ground state. For many exchanging systems it is not the case that $R_{avg}/k_{EG} > 1$, at least for some of the spins, in which case the transferred magnetization (E to G) is only partially saturated [i.e., $f(T_{EX}) \neq 0$].

CEST Experiment for Studies of Slowly Exchanging, Highly Skewed Protein Systems. Figure 2 shows the gradient-coherence-selected, enhanced-sensitivity-based pulse scheme for quantifying the exchange parameters and excited-state chemical shifts in slowly exchanging ^{15}N-labeled protein systems. The basic pulse scheme is essentially a modification of the standard experiment used to measure ^{15}N R_1 values in amide groups of proteins;[50] only the salient features as they pertain to the CEST experiment will be described here. The magnetization transfer pathway is summarized succinctly as

$$\begin{aligned} {}^1H_z(a) \rightarrow {}^{15}N_z(b) &\xrightarrow{T_{EX}} {}^{15}N_z(c) \\ &\rightarrow {}^{15}N_x(d) \xrightarrow{t_1/\mathrm{SE-RINEPT}} {}^1H_{x/y}(e) \end{aligned} \tag{3}$$

Briefly, the amide proton z magnetization at point a is transferred via a refocused INEPT element[51] to ^{15}N longitudinal magnetization at point b. The ^{1}H and ^{15}N carriers, originally on the water ^{1}H resonance and in the middle of the amide ^{15}N spectrum, respectively, are positioned in the center of the amide ^{1}H region and at the desired position for weak ^{15}N irradiation during the subsequent T_{EX} period. ^{1}H composite pulse decoupling is applied during this interval, effectively reducing the ^{15}N−^{1}H spin system to an isolated ^{15}N spin. At the end of the T_{EX} period (point c), the ^{1}H and ^{15}N carriers are returned to their original positions, and the ^{15}N transverse magnetization evolves during the subsequent t_1 period followed by transfer to ^{1}H for detection during t_2. The intensities of the cross-peaks in the resulting 2D ^{15}N−^{1}H spectra are quantified to obtain the exchange parameters and excited-state ^{15}N chemical shifts as described later. The basic pulse scheme is similar to that recently used in a study of Aβ peptide protofibril exchange dynamics,[35] except that significantly larger ^{15}N B_1 "saturating" fields were used there ($\nu_1 \approx 170$ Hz vs 5−50 Hz in the present work) with ^{15}N TROSY/anti-TROSY components[52,53] interconverted through the application of ^{1}H 180° pulses at 100 ms intervals. In cases where excited-state chemical shifts are to be measured, it is preferable to use very weak B_1 fields, since the peak line widths increase with B_1 (see below). ^{1}H decoupling is more critical in these cases because $\nu_1 \ll J_{HN}$, where J_{HN} is the

dx.doi.org/10.1021/ja3001419 | J. Am. Chem. Soc. 2012, 134, 8148−8161

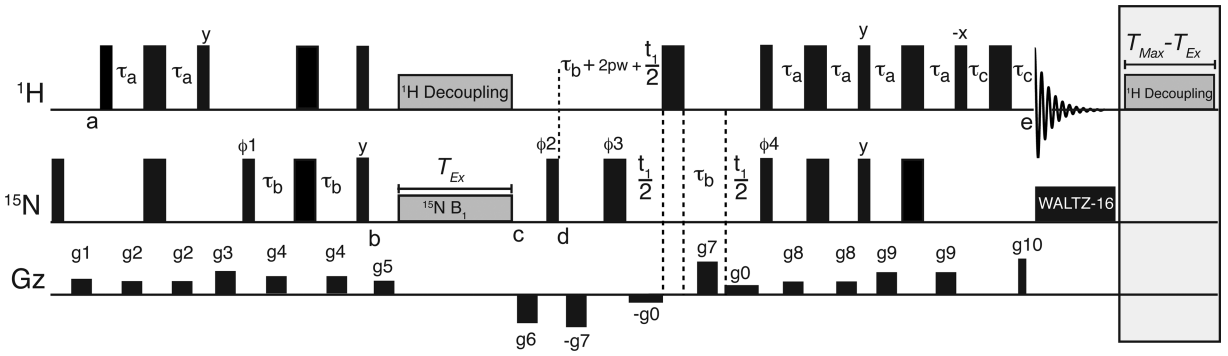

Figure 2. Pulse scheme for the weak B_1 CEST experiment for studying slow-time-scale chemical exchange at ^{15}N sites in the backbone amide groups of proteins. ^{1}H and ^{15}N 90° and 180° pulses are shown as narrow and wide black bars, respectively, and unless indicated otherwise are applied along the x axis at the maximum available power (2pw is the duration of the ^{1}H 180° pulse). The ^{1}H transmitter is positioned on the water resonance throughout the sequence except between points b and c, when it is moved to the center of the amide region (8.4 ppm). Similarly, the ^{15}N transmitter is placed at 119 ppm except between points b and c, when it is relocated to the desired offset (a set of 2D spectra are recorded with different offsets). Typical values of the ^{15}N B_1 field range between 5 and 55 Hz. A coherent decoupling train consisting of $90_x240_y90_x$ pulses[54] is used for ^{1}H decoupling between points b and c (~2.5 and ~4 kHz for 11.7 and 18.8 T, respectively). The phase cycle is $\phi_1 = \{x, -x\}$, $\phi_2 = \{y\}$, $\phi_3 = \{2x, 2y, 2(-x), 2(-y)\}$, $\phi_4 = \{x\}$, receiver = $\{x, -x, -x, x\}$ (the experiment can be performed with a minimum four-step cycle). Gradient strengths in G/cm (with corresponding lengths in ms given in parentheses) are $g_1 = 5(1)$, $g_2 = 4(0.5)$, $g_3 = 10(1)$, $g_4 = 8(0.5)$, $g_5 = 7(0.5)$, $g_6 = -25(1)$, $g_7 = 15(1.25)$, $g_8 = 4(0.5)$, $g_9 = 8(0.5)$, $g_{10} = 29.6(0.125)$. Weak bipolar gradients $g_0 = 0.1$ G/cm with opposite signs are applied during each half of the t_1 period. Quadrature detection is achieved via the enhanced-sensitivity[55] gradient method,[56,57] whereby separate data sets are acquired for each t_1 increment corresponding to (g_{10}, ϕ_4) and $(-g_{10}, -\phi_4)$. ϕ_2 and the receiver phase are incremented in a States-TPPI manner.[58] Delays are set to the following values: $\tau_a = 2.25$ ms, $\tau_b = 2.75$ ms, and $\tau_c = 0.75$ ms. ^{15}N decoupling during acquisition is achieved via WALTZ-16.[59] To ensure that heating from ^{1}H decoupling is independent of the duration of T_{EX}, ^{1}H decoupling is applied for a time $T_{MAX} - T_{EX}$ immediately after the completion of acquisition, where T_{MAX} is the maximum exchange time used. A recycle delay of 1.5 s is used between scans. A reference experiment, recorded with $T_{EX} = 0$ s, is included in fits of data so that accurate R_1^G values can be obtained.

one-bond ^{1}H−^{15}N scalar coupling constant, so the ^{15}N B_1 field by itself is not sufficient to achieve adequate decoupling.

Here we used a simple ^{1}H composite pulse decoupling scheme that was tested to ensure that decoupling sidebands would not give rise to spurious intensity dips at positions distinct from the major and minor states. Figure 3 shows results from a number of different decoupling sequences that were examined with the scheme in Figure 2 using a concentrated sample of protein L, a small 63 residue protein for which no excited states have been detected in previous work. "Intensity dips" are therefore expected only at peak positions that are measured in a regular HSQC spectrum (Figure 3A). However, standard decoupling sequences such as WALTZ-16[59] produce (small) sidebands in the decoupled ^{15}N spectrum, and when the carrier of the ^{15}N B_1 field is positioned on one of these sidebands, the major-state peak is modulated, leading to intensity dips at frequencies that do not correspond to protein resonance positions (Figure 3B, arrows). This complicates interpretation of the data. Repetition of a single (composite) ^{1}H inversion pulse (no supercycling) produces sidebands $\pm 1/(2\mathrm{pw}_{INV})$ Hz from the position of the decoupled ^{15}N peak, where pw_{INV} is the length of the inversion pulse. In general, the decoupling "artifacts" are much farther from the major peak than for the WALTZ scheme. In fact, so long as the inversion pulse is short, the first sidebands can be placed far from any of the protein major (minor) peaks, ensuring that "inadvertent" excitation does not occur. We tested a pair of composite inversion pulses, $90_x180_y270_x$[59] [Figure 3C, $\mathrm{pw}_{INV} = 1.5/(^1\mathrm{H}$ field)] and $90_x240_y90_x$[54] [Figure 3D, $\mathrm{pw}_{INV} = 1.17/(^1\mathrm{H}$ field)], both of which have excellent inversion properties over bandwidths sufficiently wide for the applications considered here. Using a 2.35 kHz ^{1}H field (11.7 T B_0 field) produces sidebands $\pm 1/(2\mathrm{pw}_{INV})$ Hz from the major-state ^{15}N resonance, corresponding to ~782.5 Hz/15.5 ppm for $90_x180_y270_x$ and ~1004 Hz/20.0 ppm for $90_x240_y90_x$, leading to very small spurious peaks in some of the CEST traces (Figure 3C,D). Of the two composite pulses considered, we prefer the $90_x240_y90_x$ pulse because it is shorter and produces side bands further away from protein resonances, most often outside the ^{15}N chemical shift window. Finally, as a gauge of the level of artifacts introduced by ^{1}H decoupling, it is worth noting that we purposefully chose a test sample with a very high protein concentration (4 mM); these (tiny) artifacts will most certainly not be observed in standard samples with concentrations on the order of 1 mM.

Cross-Validation of the Methodology. In an application of CEST that is most similar to the work described here, Clore, Torchia, and co-workers used a 2D ^{15}N-based experiment to quantify the exchange between an Aβ peptide and a multi-megadalton protofibril complex.[35] Because of the very large size of the protofibril, the ^{15}N transverse relaxation rates in the bound form are extremely large, on the order of 20 000 s^{-1}, precluding measurement of bound-state chemical shifts. In the applications considered here, we wish to use 2D CEST as a complement to CPMG relaxation dispersion in cases where the dispersion experiment fails, and our goal is to obtain both exchange parameters *and* excited-state chemical shifts. The latter requirement necessitates the use of weaker B_1 fields than in other studies and effective ^{1}H decoupling schemes that efficiently collapse the ^{15}N multiplet structure, increasing both the resolution and sensitivity, without introducing decoupling sideband artifacts that can complicate interpretation of the data. Therefore, it was important to cross-validate the approach using an exchanging system where the "answer" is already known. Here we focused on a protein (Abp1p SH3 domain)−ligand (Ark1p peptide) exchanging system that we have used previously.[28] To a 1 mM sample of ^{15}N-labeled SH3 domain was added a small amount of unlabeled peptide, corresponding to a bound mole fraction of 0.025. Under these conditions at

dx.doi.org/10.1021/ja3001419 | J. Am. Chem. Soc. 2012, 134, 8148−8161

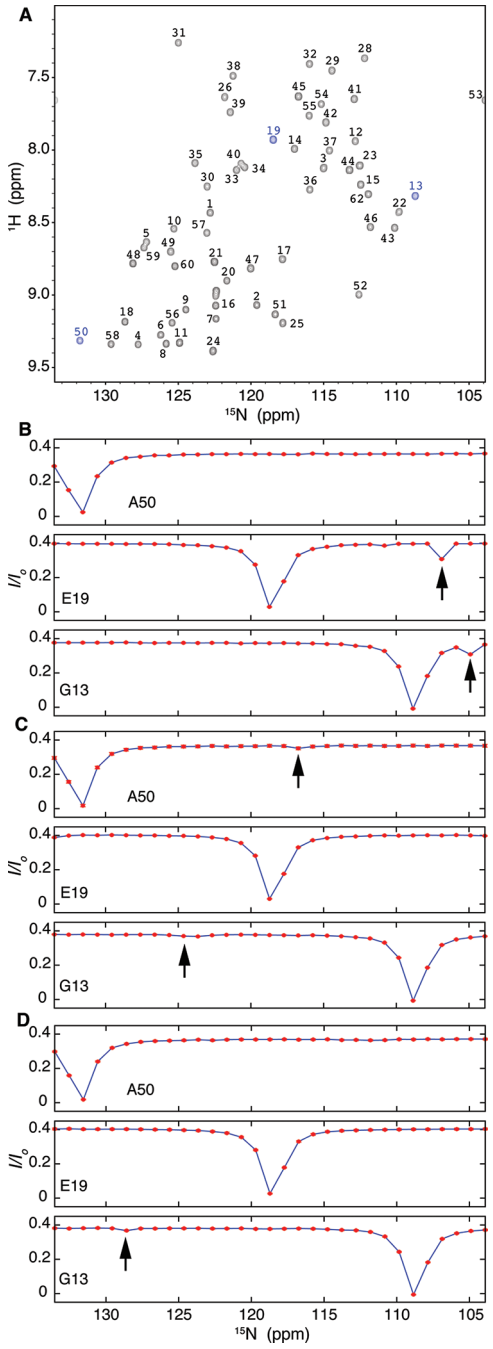

Figure 3. Elimination of ^{1}H decoupling artifacts in CEST intensity profiles. (A) Amide ^{15}N−^{1}H spectrum of protein L at 25 °C recorded at a static magnetic field strength of 11.7 T. The major dips in the intensity profiles (B, C, D) match the positions of peaks in the ^{15}N−^{1}H spectrum, corresponding to the residues indicated in the panels. Cross-peaks from residues highlighted in B−D are indicated in blue. (B) Intensity profiles obtained using WALTZ-16 ^{1}H decoupling[59] applied during the delay T_{EX} in the scheme in Figure 2 show large sideband artifacts indicated by arrows. (C, D) These artifacts can be reduced very substantially using composite-pulse ^{1}H decoupling consisting of a repetition of either (C) $90_x180_y270_x$[59] or (D) $90_x240_y90_x$[54] elements. A 28 Hz ^{15}N field and a 2.35 kHz ^{1}H decoupling field were used in all three experiments. In B−D, I_0 is the intensity of the cross-peak corresponding to the residue indicated in the panel for T_{EX} = 0, while I is the corresponding intensity for T_{EX} = 0.4 s in the presence of weak ^{15}N B_1 irradiation at a frequency indicated along the horizontal axis.

room temperature, the exchange rate is on the order of several hundred per second. The bound state thus serves as the invisible excited conformer, while the free form of the protein is the visible ground state. Since free and fully bound SH3 domain samples can be readily prepared, the chemical shifts in each of the two exchanging states are known very accurately from direct measurements.

The CEST experiment shown in Figure 2 was performed at three different ν_1 fields (12.8, 26.6, and 52.6 Hz) at a temperature of 1 °C with T_{EX} = 0.4 s. Among the 56 well-resolved resonances in the 2D ^{15}N−^{1}H HSQC spectrum (Figure 4A), a dip corresponding to a second state could be clearly observed in six amide ^{15}N intensity profiles (11.7 T), shown in Figure 4B for a pair of residues, Asp 15 and Asp 34. As expected, the resolution improved as the B_1 field was decreased (as seen by comparison of the traces recorded at 26.6 and 12.8 Hz). Rather than assuming a global two-state exchange process, we instead fit profiles from each of the six residues independently to a two-state model. If an additional dip, corresponding to a third state, had been observed in the CEST profiles, the data would have been fit to a three-state exchange mechanism. Excellent fits were obtained with the two-state model, as shown by the blue curves in Figure 4B, which match almost exactly the experimental data (red circles). The six fitted (k_{ex}, p_E) pairs are very similar (Figure 4C), consistent with a global two-state exchange process. Moreover, very similar reduced χ^2 values were obtained from per-residue fits (χ^2_{red} = 0.87) and a global fit of all of the data to a two-site exchange model (χ^2_{red} = 0.89). Most important, the fitted $\Delta\tilde{\omega}$ values are in excellent agreement with those obtained from direct measurements of the peak positions in ligand-free and fully bound samples (Figure 4D). Although only six residues showed well-resolved dips corresponding to the second state (blue in Figure 4D) chemical shifts for all of the excited-state residues could be obtained from data fitting (red circles). It should be noted that although for many of these residues the fitted $\Delta\tilde{\omega}$ values were small (well under 1 ppm), accurate chemical shift differences were nevertheless generated through analysis of the CEST profiles (see the Figure 4D inset and Table 1B in the Supporting Information). The CEST methodology can thus be used in cases where subtle conformational changes occur, corresponding to relatively small changes in chemical shifts, although it is useful to have a number of well-resolved dips corresponding to substantial $\Delta\tilde{\omega}$ values for the excited state in order to obtain (k_{ex}, p_E) values that are as accurate as possible.

As a final control we compared the values k_{ex} = 130 ± 4 s^{-1} and p_E = 2.39 ± 0.04% derived from analysis of the CEST data at 1 °C with exchange parameters obtained using other methods. At 1 °C k_{ex} and p_E could not be estimated using standard CPMG experiments. We therefore recorded CPMG dispersion profiles over a temperature range extending from 10 to 25 °C, where values could be obtained and then extrapolated to 1 °C assuming that the temperature-dependent kinetics and thermodynamics can be described by the Arrhenius and van't Hoff relations, respectively. In this manner, the values k_{ex} = 154 ± 8 s^{-1} and p_E = 2.5 ± 0.4% were obtained, and very similar values of k_{ex} = 150 ± 10 s^{-1} and p_E = 2.6 ± 0.1% were generated from a combined analysis of CPMG/D-evolution data[12] recorded at 5 °C. It is clear that very precise and accurate p_E, k_{ex}, and $\Delta\tilde{\omega}$ values can be obtained from the CEST experiment.

dx.doi.org/10.1021/ja3001419 | J. Am. Chem. Soc. 2012, 134, 8148−8161

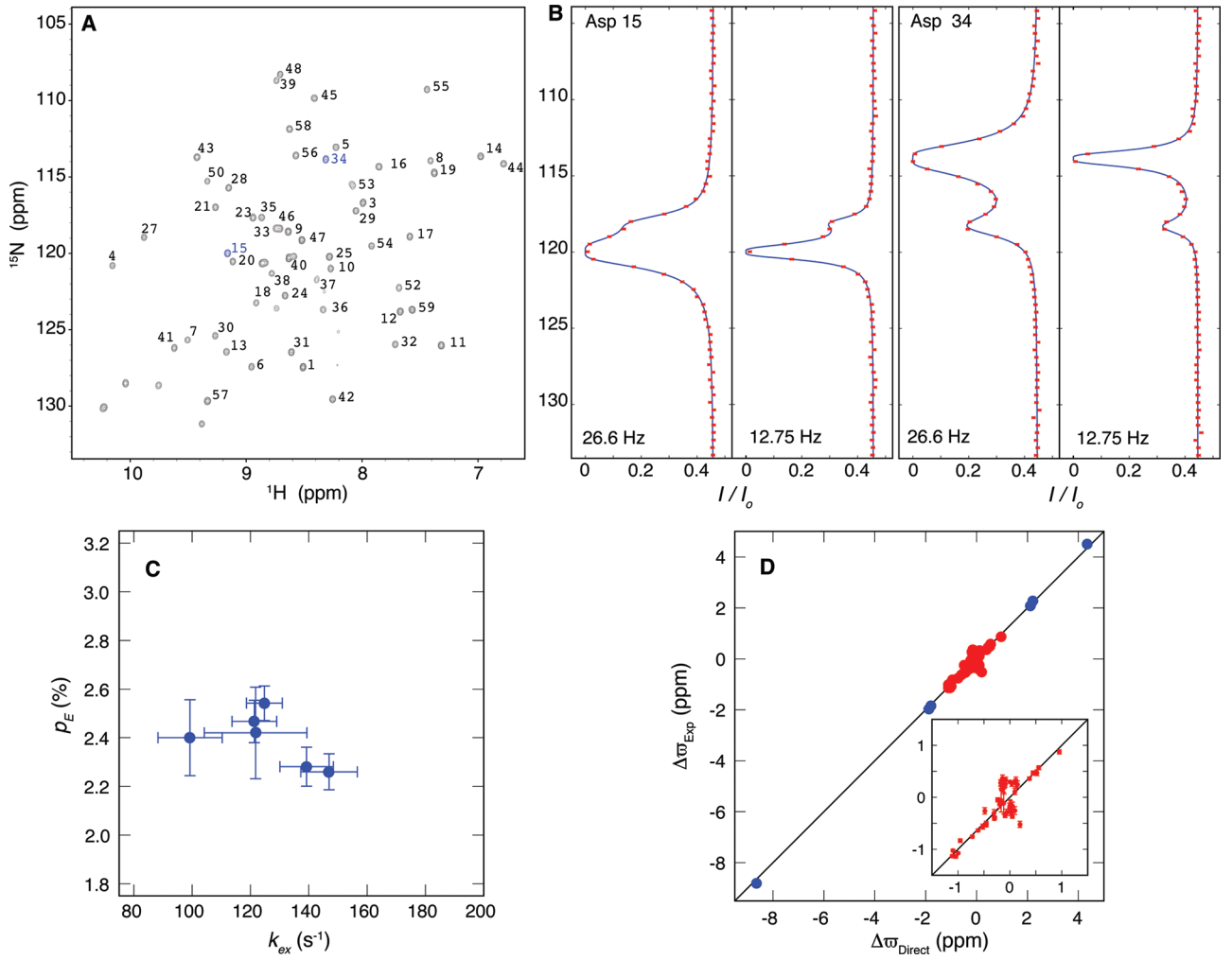

Figure 4. Validation of the methodology using a protein–ligand exchanging system (Abp1p SH3 domain, Ark1p peptide) to establish that accurate values of k_{ex}, p_E, and excited-state chemical shifts can be obtained with the CEST methodology. (A) ^{15}N–^{1}H HSQC spectrum of the Abp1p SH3 domain at 1 °C and 11.7 T. The sample contained ~2.5 mol % Arpk1p peptide, but the bound state was not observed. (B) Intensity profiles for Asp 15 and 34 for ν_1 = 26.6 and 12.75 Hz and T_{EX} = 0.4 s, where I (I_0) is the intensity of the major-state correlation in the presence (absence) of 0.4 s B_1 irradiation. The main dip is at the resonance frequency of the major state, while the second smaller dip corresponds to the invisible minor state. Experimental data points are in red, and the blue continuous lines correspond to the best (global) fit of the data. (C) Distribution of (k_{ex}, p_E) values obtained from single-residue fits for each of the six residues that showed a well-resolved dip corresponding to the excited state. (D) $\Delta\tilde{\omega}$ values obtained from fits of CEST profiles ($\Delta\tilde{\omega}_{Exp}$) are in excellent agreement with the values measured directly from ligand-free and fully bound SH3 domain samples ($\Delta\tilde{\omega}_{Direct}$). Points in blue correspond to the six residues in (C) and those in red to the remaining residues; a total of 56 residues were analyzed, corresponding to the number of ground-state peaks that could be accurately quantified in the ^{1}H–^{15}N HSQC spectrum. The inset shows an expansion of the region centered around 0 ppm, illustrating that accurate values of $\Delta\tilde{\omega}$ were obtained even for small chemical shift differences. In all of the analyses, profiles corresponding to ν_1 = 52.6, 26.6, and 12.75 Hz were fit simultaneously.

Folding of the A39G Mutant of the FF Domain from HYPA/FBP11. The four-helix bundle FF domain from human HYPA/FBP11 folds via a compact intermediate.[43] The rate-limiting intermediate to native-state transition for the wild-type FF domain has been studied extensively by CPMG relaxation dispersion NMR spectroscopy, leading to an atomic-resolution structure of the intermediate state.[11,60] It shows that a large number of non-native interactions are formed along the folding pathway that serve as kinetic traps. In an effort to understand the effects of mutations on the structure of the intermediate and on the relation between this structure and the folding kinetics, we initiated a series of studies exploring the folding and structural properties of single-point mutants of the FF domain. One such mutant is the A39G substitution, which was shown by stopped-flow fluorescence to decrease the folding rate significantly.[43] Only very small ^{15}N dispersion profiles were obtained from initial CPMG relaxation dispersion NMR studies at 1 °C, complicating the extraction of accurate exchange parameters and chemical shifts (see below). In contrast, CEST experiments recorded on the A39G mutant (Figure 5) clearly "detected" chemical exchange, with profiles from 37 residues showing clear evidence of another state (Figure 5B). The (k_{ex}, p_E) points extracted from per-residue fits of profiles recorded at three ν_1 fields (26.2, 13, and 6.2 Hz) with T_{EX} = 0.5 s clustered into a single group, strongly suggesting a global two-state exchange process (Figure 5C). The values k_{ex} = 51.6 ± 1 s^{-1} and p_E = 1.65 ± 0.02% were obtained from a global fit of all of the CEST data to a two-state exchange model, and the value of χ^2_{red} obtained, 0.97, is very similar to the χ^2_{red} value of 0.98 measured from the individual residue fits.

Even at an initial stage of analysis, excited-state chemical shifts contain useful structural information.[18,61] For example, the fitted $\Delta\tilde{\omega}$ values correlate very well with the difference

dx.doi.org/10.1021/ja3001419 | J. Am. Chem. Soc. 2012, 134, 8148–8161

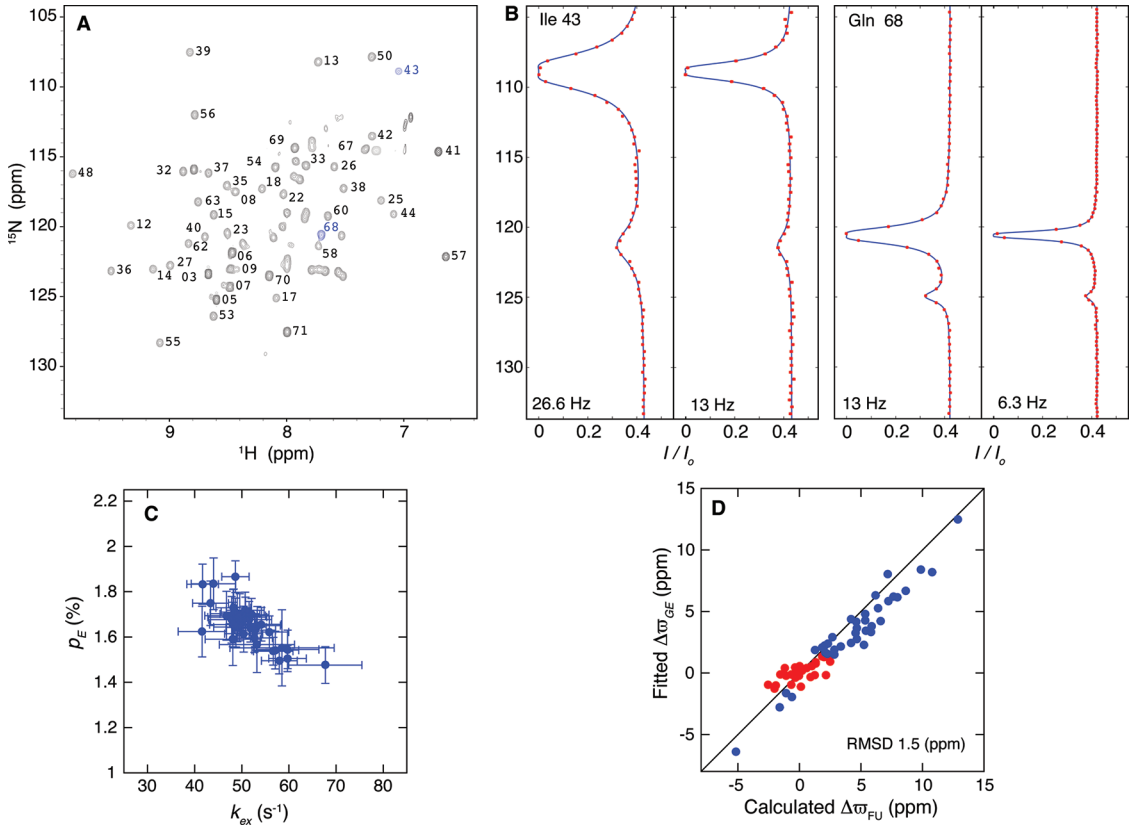

Figure 5. Detection and characterization of the invisible excited state of the A39G FF domain by CEST. (A) ^{15}N−^{1}H HSQC spectrum of the A39G FF domain at 1 °C and 11.7 T; only cross-peaks from the native state of the protein are visible. (B) Intensity profiles for Ile 43 and Gln 68 recorded at the indicated ^{15}N B_1 field strengths. In each of the profiles a dip corresponding to the position of the minor-state correlation can be seen in addition to the expected dip for the major state. The width of each peak is a function of the line width of the resonance and the B_1 field strength. (C) Very similar k_{ex} and p_E values were obtained from per-residue fits of the intensity profiles for 37 amino acids showing clear evidence of a second state. Data at three ^{15}N B_1 fields (26.2, 13.0, and 6.2 Hz) were used in the fits. (D) Comparison of the fitted $\Delta\tilde{\omega}$ values with those expected for a folding transition, with the unfolded ^{15}N chemical shifts predicted using the method of Tamiola et al.[64] Values of chemical shifts and exchange parameters were obtained from a global fit of all of the data for the 37 residues for which a second state was observed (blue); excited-state shifts were subsequently obtained for the remaining residues (red) using (k_{ex}, p_E) values fixed to those from the global fit involving the 37 residues. In total, $\Delta\tilde{\omega}$ values were obtained for 64 residues (red + blue), including many residues for which $\Delta\tilde{\omega}$ < 0.5 ppm (see Table 2B in the Supporting Information).

between the predicted unfolded state chemical shifts and those for the native conformer (Figure 5D), establishing that the excited state monitored by the CEST experiments is unfolded. Previous studies of the wild-type FF domain have established that folding proceeds via an on-pathway intermediate[62] and that it is best described in terms of a three-state exchange process. CPMG relaxation dispersion studies of the wild-type protein indicated that the population of the unfolded state was significantly lower than that of the intermediate state (by ∼10-fold at 30 °C), so it could effectively be neglected in the analysis of the dispersion data.[11] The results of the CEST experiments presented here may indicate that the relative populations of the unfolded and intermediate states of the A39G FF domain at 1 °C are reversed relative to the wild-type domain at 30 °C, since the excited state observed corresponds to an unfolded ensemble. However, this cannot be concluded unequivocally. As pointed out by Clore et al. in another context[63] it may be that the time scale of exchange between the folded and unfolded states of the A39G FF domain is optimal for the observation of the CEST effect, while exchange with the intermediate state is sufficiently fast that additional dips cannot be observed (see below), irrespective of the relative populations of the unfolded and intermediate states. It is worth noting that because (k_{ex}, p_E) values can be extracted on a per-residue basis, the fact that they cluster (Figure 5C) provides strong evidence that the CEST profiles derive from a common exchange process.

In addition to chemical shifts, excited-state transverse relaxation rates can also be determined from fits of the CEST data, as demonstrated previously in studies of Aβ peptide−fiber exchange.[35] In the case of the A39G FF mutant considered here, it is clear that there are differences between transverse relaxation rates for different residues, as can be seen in a comparison of the traces for Ile 43 and Gln 68 (Figure 5B).

Notably, consistently higher fitted ^{15}N transverse relaxation rates were observed for the excited state relative to the native ground state (Figure 6A). This is a surprising result since the unfolded structural ensemble is expected to be more flexible than the native conformer, which should lead to lower rather than higher rates.[65] It is worth noting that the transverse rates were fitted under the assumption of two-state exchange and did not contain contributions from the exchange event that was fit, but they most certainly would be affected by any other exchange processes that may have been present. For example, if the unfolded ensemble exchanges with a conformer that is distinct from the native structure, then elevated R_2^E rates reflecting the additional exchange process would be obtained. In this case, the exchange contribution to R_2^E from this third process, R_{ex}^E, would be expected to scale with the static magnetic field as B_0^n, with $0 \leq n \leq 2$. Sites with relatively small R_{ex}^E rates from the additional exchange process, corresponding to small

dx.doi.org/10.1021/ja3001419 | J. Am. Chem. Soc. 2012, 134, 8148−8161

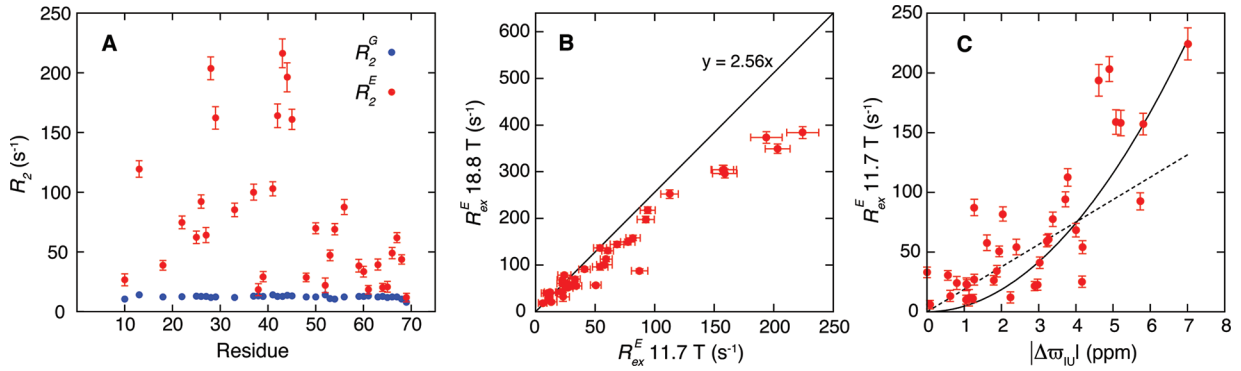

Figure 6. The invisible unfolded state of the A39G FF domain exchanges on a micro-to-millisecond time scale with another sparsely populated invisible state. (A) Ground (R_2^G)- and excited (R_2^E)-state ^{15}N transverse relaxation rates for the 37 residues showing clear evidence of a second state in CEST profiles at 1 °C and 11.7 T. Although the relaxation rates do not contain contributions from the exchange process that was fit, they are influenced by additional exchange processes. (B) Comparison of the exchange contributions to R_2^E (R_{ex}^E) recorded at 18.8 and 11.7 T; small to intermediate values of R_{ex}^E scale as the square of the ratio of the field strengths, 2.56 (see the text). All of the data recorded at the two B_0 fields were together fit to a global two-state process. (C) Correlation between the R_{ex}^E values at 11.7 T and the difference in the chemical shifts of the unfolded state and a previously characterized[11] intermediate state for the wild-type FF domain, $|\Delta\tilde{\omega}_{IU}|$. The black curve $y = 4.65x^2$ corresponds to the best quadratic fit to the data, while the best-fit linear relation $y = 18.8x$ is shown as a dashed line.

changes in chemical shift, would be in the fast-exchange limit, with $n = 2$. In contrast, residues with larger R_{ex}^E values would have smaller values of n, since they would not be in the fast-exchange limit. Figure 6B shows that this was observed for the R_{ex}^E values obtained from the CEST profiles recorded at 11.7 and 18.8 T. Small values of R_{ex}^E scale as the square of the ratio of the static magnetic field strengths ($18.8^2/11.7^2 = 2.56$ in the present case), while larger values scale with progressively smaller ratios. For this reason, the correlation between R_{ex}^E values measured at 18.8 and 11.7 T follows the linear relation, $y = 2.56x$ (solid line in Figure 6B) for small values of R_{ex}^E (small $\Delta\tilde{\omega}$ values corresponding to fast exchange with a third state), with a decreasing dependence as R_{ex}^E (and hence $\Delta\tilde{\omega}$) becomes larger. In this analysis, we estimated the excited-state R_{ex}^E values as $R_2^E - 0.5R_2^G$, where we assumed that the intrinsic R_2 of the unfolded state is approximately half that of the folded state.[65]

What then is the origin of the third state? Figure 6C plots fitted R_{ex}^E values from the CEST profiles of the A39G FF domain (11.7 T) versus the difference in the ^{15}N chemical shifts of the intermediate and unfolded states, $\Delta\tilde{\omega}_{IU}$, determined in a previous study of the wild-type FF domain.[11] If the third state is indeed the previously characterized intermediate and the exchange between the unfolded and intermediate states is reasonably fast on the NMR chemical shift time scale, then a strong correlation between R_{ex}^E and $\Delta\tilde{\omega}_{IU}^2$ should be observed. In this regard, it is worth noting that both stopped-flow fluorescence and CPMG dispersion studies have shown that the intermediate exchanges rapidly with the unfolded ensemble ($k_{ex}^{FI} \ll k_{ex}^{IU}$),[11,43] so a quadratic dependence is a reasonable first model. The solid curve in Figure 6C shows a modest correlation assuming a quadratic dependence (certainly much better than that for a linear correlation, shown by the dashed line), suggesting that the third state may be structurally related to the intermediate that has been studied previously in the wild-type protein[11] and the L24A FF domain mutant.[60] However, additional studies must be undertaken to characterize further this additional exchanging conformer.

It is of interest to compare the exchange parameters and chemical shift differences extracted from fits of CPMG relaxation dispersion and CEST data, especially since the A39G FF domain is a challenging case with small dispersion profiles. A previous study of the Abp1p SH3 domain−Ark1p peptide exchanging system as a function of temperature established that as exchange rates decrease, the accuracy of the extracted (k_{ex}, p_E) values becomes poor, as was also noted in simulations.[12] Of course, dispersion profiles are sensitive only to the $p_E k_{ex}$ product in the slow-exchange limit. We recorded CPMG dispersion profiles at 11.7, 14.0, and 18.8 T (Figure 7A,B) and fit the dispersion profiles globally to a two-site

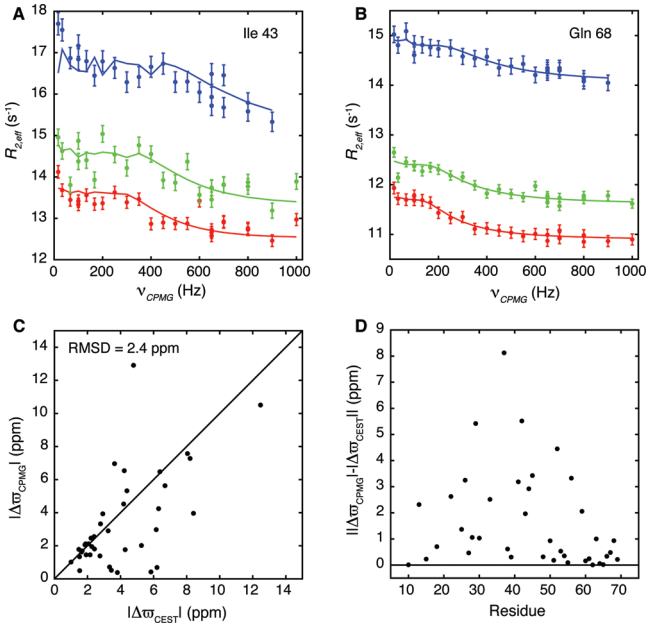

Figure 7. (A, B) ^{15}N CPMG relaxation dispersion profiles for a pair of residues of the A39G FF domain at 1 °C and 11.7 T (red), 14.0 T (green), and 18.8 T (blue), along with best fits of dispersion profiles (solid lines) obtained from simultaneous analysis of all of the data, as described previously.[18] (C) Linear correlation plot of $|\Delta\tilde{\omega}_{CPMG}|$ vs $|\Delta\tilde{\omega}_{CEST}|$, along with the solid line representing $|\Delta\tilde{\omega}_{CPMG}| = |\Delta\tilde{\omega}_{CEST}|$; a pairwise rmsd of 2.4 ppm was obtained. (D) Plot of $||\Delta\tilde{\omega}_{CPMG}| - |\Delta\tilde{\omega}_{CEST}||$ vs residue number. The horizontal line corresponding to $|\Delta\tilde{\omega}_{CPMG}| - |\Delta\tilde{\omega}_{CEST}| = 0$ is also shown.

dx.doi.org/10.1021/ja3001419 | J. Am. Chem. Soc. 2012, 134, 8148−8161

exchange model as described previously.[18] The exchange parameters, (k_{ex}, p_E) = (101 ± 18 s^{-1}, 0.8 ± 0.1%), do not agree with the values (51.6 ± 1 s^{-1}, 1.65 ± 0.02%) extracted from the CEST fits, although the value of $p_E k_{ex}$ is reasonably accurate, in keeping with expectations in the slow-exchange limit. Figure 7C plots the $|\Delta\tilde{\omega}|$ values extracted from separate analyses of CPMG ($|\Delta\tilde{\omega}_{CPMG}|$) and CEST ($|\Delta\tilde{\omega}_{CEST}|$) data, and Figure 7D shows the difference $||\Delta\tilde{\omega}_{CPMG}| - |\Delta\tilde{\omega}_{CEST}||$ as a function of residue number. It is clear that there are substantial deviations [pairwise root-mean-square deviation (rmsd) of 2.4 ppm]. These differences may in part arise from the fact that the dispersion profiles are sensitive to the third state that was inferred from CEST data on the basis of the substantial R_{ex}^E values for some of the backbone ^{15}N nuclei of the A39G FF domain, although this is hard to establish given the small size of the CPMG profiles. It may be possible to perform a combined analysis of the CEST and CPMG data to obtain a more complete description of the exchange reaction, although we have not done so here.

Range of Time Scales That Can Be Characterized. To evaluate the utility of the experiment more fully, we generated synthetic data sets for a pair of k_{ex} values, 20 and 200 s^{-1}, with p_E = 1.5% and a static magnetic field strength of 11.7 T. To keep the simulations as realistic as possible, we used 37 "residues" corresponding to those fit from the A39G FF domain with parameters $\{\Delta\tilde{\omega}_{GE}, R_1^G, R_2^G, R_2^E\}$ taken from the experimental fits; these residues showed clear evidence of a second state in the experimental CEST profiles. CEST data were simulated for four ν_1 fields (see the Figure 8 caption), and a Gaussian error based on the experimental error was randomly added to each calculated intensity point. We fit each residue independently using profiles from all four ν_1 fields, and the distribution of (k_{ex}, p_E) points obtained for the 24 residues with $|\Delta\tilde{\omega}_{GE}| > 2.5$ ppm is shown in Figure 8. When k_{ex} was set to 200 s^{-1}, extremely accurate exchange parameters were obtained (Figure 8A), with k_{ex} and p_E values (mean ± standard deviation) of 195 ± 7 s^{-1} and 1.47 ± 0.02%, respectively. A global fit including all 37 residues yielded k_{ex} = 192.5 ± 1.5 s^{-1} and p_E = 1.46 ± 0.01%. The (k_{ex}, p_E) values were well-defined for k_{ex} = 20 s^{-1} as well, with fitted values of 19.2 ± 3.3 s^{-1} and 1.4 ± 0.2% (Figure 8B). The values k_{ex} = 18.2 ± 0.5 s^{-1} and p_E = 1.48 ± 0.03% were obtained from a global fit including all 37 residues.

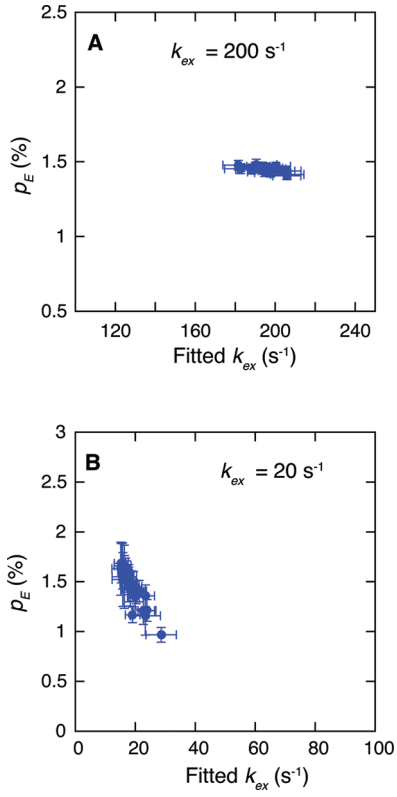

Figure 8. Computations establishing the utility of CEST for studies of slow chemical exchange. Synthetic data were generated as described in the text and fitted as per the experimental data. (A) (k_{ex}, p_E) distribution from fits of CEST profiles generated with $\{\Delta\tilde{\omega}_{GE}, R_1^G, R_2^G, R_2^E\}$ values taken from the experimental fits of 37 residues for the A39G FF domain that showed distinct dips for the ground and excited states. Values of k_{ex} = 200 s^{-1} and p_E = 1.5% were assumed, and the CEST data were simulated (and then simultaneously fit) for four different B_1 fields corresponding to frequencies of 50, 25, 12.5, and 6.25 Hz with T_{EX} = 0.4 s. (B) As in (A) but with k_{ex} = 20 s^{-1} and data simulated for 25, 16, 11, and 6 Hz with T_{EX} = 0.8s.

CONCLUDING REMARKS

Over the past decade, a significant number of NMR methods for studying excited protein states have been developed. These include CPMG relaxation dispersion[45] and D-evolution[12] approaches for characterizing exchanging systems in the approximate regime 200 $s^{-1} \leq k_{ex} \leq$ 2000 s^{-1}; $R_{1\rho}$ experiments,[66] which extend the exchange time scale to higher rates with upper bounds on the order of 50 000 s^{-1}; and paramagnetic relaxation enhancement measurements, which are most powerful for systems in the fast-exchange regime.[7] Notably, excited states with interconversion rates on the order of ~200 s^{-1} or lower have, in general, remained elusive because the slower exchange translates into a smaller effect on the observable ground state. We have shown here that the CEST experiment provides an extremely sensitive and robust approach for obtaining exchange parameters and line widths in the excited state and, most important for the structural work in which we are interested, for measuring accurate excited-state chemical shift values precisely in the slow-exchange limit of interest. Central to the utility of the method is that the experiment, unlike dispersion-based approaches, relies on longitudinal rather than transverse relaxation, with the former often being more than an order of magnitude slower. This enables longer mixing periods to be employed, leading to a "buildup" of the effect of exchange, even in cases where the exchange rates are low. It also facilitates applications to larger protein systems, since for macromolecules such as proteins, T_1 values increase as a function of molecular weight. Although T_2 values decrease for larger systems, it is important to realize that the major contributor to the line width of the dips in the CEST spectra is the B_1 field strength, with the effective line width increasing with applied field. It is possible to decrease the contributions from the intrinsic line width by implementing a TROSY[52] version of the experiment. It is worth noting in this regard that relatively large R_2^E values were observed for many of the ^{15}N spins in the FF domain excited state (R_2^E > 50 s^{-1}), yet accurate values of $\Delta\tilde{\omega}$ could be obtained. Studies at higher static magnetic fields should also be advantageous, since $\Delta\omega$ values increase linearly while T_1 values increase quadratically with the field in applications involving large molecules.

The utility of the CEST experiment has been demonstrated for two experimental systems with k_{ex} values of ~50 and ~150 s^{-1}

dx.doi.org/10.1021/ja3001419 | J. Am. Chem. Soc. 2012, 134, 8148–8161

and by simulations for k_{ex} values ranging from 20 to 200 s^{-1} showing that accurate exchange parameters and chemical shifts can be obtained even from fits on a per-residue basis. On a practical note, we suggest that when a system is investigated for the first time, a relatively high ν_1 value (25−50 Hz) should be employed along with a long mixing time, T_{EX}, in order to facilitate the detection of excited states. Once such states are observed, experiments can be performed at multiple B_1 field strengths. Single-residue fits require data recorded at no less than a pair of B_1 field strengths, and low fields have the advantage that narrower lines are obtained, albeit often at the expense of smaller effects.

As a final note, it is worth comparing the advantages of CEST to the magnetization exchange transfer approach for quantifying slowly exchanging protein systems.[32,67−70] Here longitudinal magnetization is transferred between states during a mixing time that is placed between pairs of chemical shift evolution periods (t_1 and t_2 in a 2D data set), leading in favorable cases to the observation of cross-peaks connecting correlations derived from interconverting sites. The time dependencies of the evolution of cross- and diagonal peaks are subsequently fit to extract exchange parameters. For a two-site exchanging system it is straightforward to show that the maximum intensity of the cross-peaks is less than $p_G \times p_E$, placing a rather severe restriction on what the minimum value of p_E must be so that quantifiable cross-peaks can be obtained. Only one or two exchange cross-peaks could be reliably identified in magnetization exchange spectra recorded on either of the SH3 (p_E = 2.4%) or FF (p_E = 1.7%) domains considered here, so this approach for quantifying exchange and obtaining chemical shifts of the excited state was not an option. In contrast, in the CEST experiment, application of a radio frequency field at the position of the minor-state correlation for a mixing period of several hundreds of milliseconds leads to a very significant amplification effect that substantially improves the sensitivity of the experiment relative to magnetization exchange.[37] As a result, and unlike magnetization exchange experiments, it is not a requirement that excited-state correlations be observed in the spectra. Furthermore, because "typical" HSQC data sets are analyzed (all correlations derived from the major conformer), resolution is not nearly as limiting as in magnetization exchange experiments, where diagonal peaks from both states as well as cross-peaks must be well resolved. The results of the present study establish that CEST spectroscopy will play an important role in characterizing protein excited states that exchange in the slow regime, providing a complement to CPMG relaxation dispersion. Robust excited-state chemical shifts are available from fits of CEST data, in many cases simply by inspection, facilitating structural studies of rare conformers and significantly increasing the exchange time-scale window that is amenable to detailed study by experimental NMR spectroscopy.

MATERIALS AND METHODS

NMR Samples. A [U-^{15}N,^{2}H]-labeled protein L sample dissolved in 50 mM sodium phosphate, 0.05% NaN_3, 10% D_2O buffer (pH 6.0) was prepared as described previously.[71] The sample was very concentrated (~4 mM) to test for experimental artifacts (see the text). An Abp1p SH3 domain exchanging complex was produced in a manner discussed previously,[28] comprising ~1.5 mM [U-^{15}N,^{2}H]-labeled Abplp SH3 domain and unlabeled Ark1p peptide (17 residues) in a 50 mM sodium phosphate, 100 mM NaCl, 1 mM EDTA, 1 mM NaN_3, 10% D_2O buffer (pH 7.0). The concentration of added peptide was such that the sample was 97.5% free, 2.5% peptide-bound. A second Abp1p−Ark1p sample, fully bound, was prepared for direct measurements of chemical shifts in the bound state. The A39G FF domain was expressed and purified as described previously for other FF variants.[11,43] The sample consisted of ~2 mM [U-^{15}N]-labeled protein dissolved in a 50 mM sodium acetate, 100 mM NaCl, 10% D_2O buffer (pH 5.7).

NMR Spectroscopy. Experiments were performed on Varian Inova spectrometers (11.7 and 18.8 T) equipped with room-temperature triple resonance probes. The weak ^{15}N B_1 field (applied during T_{EX}) was calibrated in a 1D fashion using the approach of Guenneugues et al.[72] with the pulse sequence shown in Figure 2 by focusing on an isolated protein peak that did not show exchange broadening. The measured inhomogeneity was ~10% at both 11.7 and 18.8 T and relatively constant over the range of B_1 values used in the experiments.

All of the experiments involving protein L were performed at 25 °C, 11.7 T, and ν_1 = 28 Hz with a ^{1}H decoupling field strength of 2.35 kHz during T_{EX} = 0.4 s (see Figure 2). A series of 31 2D data sets were acquired, corresponding to ^{15}N offsets between 103.91 and 133.52 ppm, obtained at 50 Hz (0.987 ppm) intervals.

Experiments on the Abp1p−Ark1p system were recorded at 1 °C and 11.7 T. Sixty 2D data sets were obtained, with the ^{15}N carrier centered at frequencies corresponding to 104.16 to 133.81 ppm at a spacing of 25 Hz (0.494 ppm) during T_{EX} = 0.4 s. A pair of ^{15}N B_1 fields corresponding to field strengths of 12.8 and 26.6 Hz were used. Data at a third field strength (52.6 Hz) were recorded; here a spacing of 30 Hz (0.593 ppm) was employed. In all of the experiments, ^{1}H decoupling during T_{EX} was achieved using a 2.3 kHz field with composite pulse decoupling consisting of repeated applications of a $90_x240_y90_x$ element. Each 2D data set was recorded with acquisition times of (33 ms, 64 ms), eight transients, and a delay of 1.5 s between scans, corresponding to 19 h (ν_1 = 12.8, 26.6 Hz) and 16 h (ν_1 = 52.6 Hz) for each complete series.

CEST experiments were performed on the A39G FF domain at 1 °C and 11.7 or 18.8 T. Data recorded at 11.7 T comprised a series of 2D spectra with ^{15}N offsets ranging between 104.16 and 133.81 ppm obtained in increments of 0.494 ppm (25 Hz) for ν_1 fields of 26.2 and 13 Hz and 0.296 ppm (15 Hz) when the B_1 field was 6.2 Hz. Acquisition times of (35.6 ms, 64 ms) in (t_1, t_2) were used, along with eight transients per free induction decay (FID) and a relaxation delay between scans of 1.5 s for total data collection times of 20 h (ν_1 = 26.2 and 13 Hz) and 33 h (ν_1 = 6.2 Hz). A T_{EX} value of 500 ms was used for all of the experiments, with a 2.46 kHz ^{1}H decoupling field ($90_x240_y90_x$). CEST experiments were performed at 18.8 T using a 3.67 kHz ^{1}H decoupling field, ν_1 = 14.8 or 28.9 Hz, and T_{EX} = 500 ms. ^{15}N carrier frequencies were positioned from 104.36 to 133.96 ppm in steps of 0.3085 ppm (25 Hz). Similar acquisition parameters were used as described for data acquired at 11.7 T, except that four transients per FID were recorded, for a total acquisition time of 19.5 h for each data set.

CPMG relaxation dispersion profiles[13] were recorded at 11.7, 14.0, and 18.8 T as described previously,[73] using a constant-time CPMG interval[26] (60 ms) with ^{1}H continuous-wave decoupling along with 25 ν_{CPMG} values ranging from 17 to 1000 Hz, with three duplicate points for error analysis. Dispersion data from all static magnetic field strengths were analyzed simulataneously.

Data Processing and Analysis. All of the data sets were processed using the NMRpipe program,[74] with peak intensities quantified using FuDA;[75] subsequently, the spectra were visualized using SPARKY.[76] CPMG relaxation data were analyzed in the standard manner using the program CATIA,[75] which numerically propagates the Bloch−McConnell equations.[77] Errors in the CPMG data were estimated on the basis of 2−3 repeat measurements. Errors in the CEST intensity profiles were estimated on the basis of the scatter in regions of 1D profiles that did not contain any intensity dips. The CEST intensity profiles were analyzed using an in-house-written python program, ChemEx (available upon request), that minimizes the standard χ^2 equation

$$\chi^2(\xi) = \sum_{i=1}^{N} \left(\frac{I_i^{\text{exptl}} - I_i^{\text{calcd}}(\xi)}{\sigma_i^{\text{exptl}}} \right)^2 \quad (4)$$

In eq 4, the summation extends over all the desired experimental points, σ^{exptl} is the error in the experimental intensity I^{exptl}, I^{calcd} is the calculated intensity, and $\xi = \{x_1, ..., x_n\}$ refers to the different fitting parameters. The value of σ^{exptl} was estimated on the basis of noise in the regions of spectra that did not contain any intensity dips, with the minimum error set to the median error of all the residues. Intensities were calculated using the Bloch–McConnell equations[77] for a single spin-$^1/_2$ particle exchanging between two states G and E with rate constants k_{GE} and k_{EG}:

$$\frac{d}{dt}\begin{pmatrix} E/2 \\ I_x^G \\ I_y^G \\ I_z^G \\ I_x^E \\ I_y^E \\ I_z^E \end{pmatrix} = \begin{pmatrix} 0 & 0 & 0 & 0 & 0 & 0 & 0 \\ 0 & -R_2^G - k_{GE} & -\omega_G & \omega_1 & k_{EG} & 0 & 0 \\ 0 & \omega_G & -R_2^G - k_{GE} & 0 & 0 & k_{EG} & 0 \\ 2R_1^G I_{eq}^G & -\omega_1 & 0 & -R_1^G - k_{GE} & 0 & 0 & k_{EG} \\ 0 & k_{GE} & 0 & 0 & -R_2^E - k_{EG} & -\omega_E & \omega_1 \\ 0 & 0 & k_{GE} & 0 & \omega_E & -R_2^E - k_{EG} & 0 \\ 2R_1^E I_{eq}^E & 0 & 0 & k_{GE} & -\omega_1 & 0 & -R_1^E - k_{EG} \end{pmatrix} \begin{pmatrix} E/2 \\ I_x^G \\ I_y^G \\ I_z^G \\ I_x^E \\ I_y^E \\ I_z^E \end{pmatrix} \quad (5)$$

In eq 5, E is the identity operator, I_j^K is component $j \in \{x, y, z\}$ of the angular momentum for state K $\in$ {G, E}, R_q^K is a spin–lattice ($q = 1$) or spin–spin ($q = 2$) relaxation rate, ω_G and ω_E are the offsets (in rad/s) of the weak ^{15}N irradiation field from states G and E (ω_G is obtained from the ground-state peak position and is not a fitting parameter). I_{eq}^G and I_{eq}^E are the equilibrium populations of states G and E, respectively; the value of I_z^G is calculated by solving eq 5 (subject to the appropriate set of initial conditions) as a function of the field offset B_1. To mimic the phase cycling of ϕ_1 (Figure 2), two sets of initial conditions, namely, $I_{x,y}^{G/E} = 0$, $I_z^G = p_G$, $I_z^E = p_E$ and $I_{x,y}^{G/E} = 0$, $I_z^G = -p_G$, $I_z^E = -p_E$, were used in all of the calculations, and the difference in I_z^G obtained in the two cases was retained. B_1 field inhomogeneity was taken into account by performing 10 calculations with different B_1 fields evenly spaced between $\pm 2\sigma$ around the mean, where σ is the standard deviation of the measured B_1 field distribution. The 10 calculations were averaged using coefficients that assumed a Gaussian profile. The data could not constrain R_1^E because the molecules spend very little time in state E, so we assumed $R_1^G = R_1^E$; using 0.1 $s^{-1} \le R_1^E \le 4$ s^{-1} had no effect on the results. The fitting parameters are k_{ex}, p_E, $\tilde{\omega}_E$, R_1^G, R_2^G, R_2^E, and a residue-specific initial intensity I_0. It should be noted that k_{ex} and p_E are residue-specific in the case of single-residue fits but global fitting parameters common to all of the residues in the case of multiresidue fits; R_1^G, R_2^G, and R_2^E are residue-specific and dependent on the magnetic field strength B_0; and is $\tilde{\omega}_E$ residue-specific but independent of B_0. In principle, it is possible to measure R_1^G and R_2^G in independent experiments and fix these parameters in fits of the CEST data to values obtained using other pulse schemes. We prefer, however, not to do this. First, in addition to recording a series of experiments with different positions of the B_1 field applied for a time T_{EX}, we also record an additional data set with $T_{EX} = 0$. These data sets determine R_1^G accurately because $\ln(I) = \ln(I_0) - R_1^G T_{EX}$, where I is the intensity of the ground-state correlation when the B_1 field is applied at a position far removed from the ground- and excited-state peaks (so that they are not affected) and I_0 is the intensity when $T_{EX} = 0$. Second, when R_1^G and R_2^G are estimated using separate experiments, there is always a worry that what is measured is slightly different than in the CEST data set and that the differences could potentially translate into errors in the exchange parameters.

As described above, the data were fit using the initial conditions $I_z^G = \pm p_G$ and $I_z^E = \pm p_E$. We also fit the data taking into account relaxation during magnetization transfer from ^{1}H to ^{15}N in the scheme shown in Figure 2 (between points *a* and *b*). This could only be done in an approximate manner because we did not have an estimate for the transverse relaxation rates of the amide protons, including contributions from chemical exchange. We therefore assumed identical relaxation decays during each of the two INEPT elements preceding the CEST period. In a separate analysis of the data, we assumed the initial condition $I_z^E = 0$. In all cases, the extracted parameters were affected only very little by the assumptions used. For residues with substantial contributions from transverse relaxation in the ground state, it is important that these be taken into account. In such cases, we recommend that amide ^{1}H transverse relaxation rates be estimated from F_2 line widths (e.g., in recorded CEST spectra) while the ^{15}N line widths are allowed to emerge naturally from fits of the data.

■ ASSOCIATED CONTENT

Supporting Information

Tables listing extracted exchange parameters and chemical shifts; sets of fitted CEST profiles for all residues used in the global fits for both the Abp1p–Ark1p and the A39G FF domain exchanging systems. This material is available free of charge via the Internet at http://pubs.acs.org.

■ AUTHOR INFORMATION

Corresponding Author

pramodh@pound.med.utoronto.ca; kay@pound.med.utoronto.ca

Author Contributions

§P.V. and G.B. contributed equally.

Notes

The authors declare no competing financial interest.

■ ACKNOWLEDGMENTS

We thank Dr. Ranjith Muhandiram for advice on the implementation of the pulse sequence and Prof. Julie Forman-Kay for providing laboratory facilities for sample preparation. G.B. acknowledges the Canadian Institutes of Health Research (CIHR) for a postdoctoral fellowship. L.E.K. holds a Canada Research Chair in Biochemistry. The work was supported by grants from the Natural Sciences and Engineering Research Council of Canada and the CIHR.

■ REFERENCES

(1) Austin, R. H.; Beeson, K. W.; Eisenstein, L.; Frauenfelder, H.; Gunsalus, I. C. *Biochemistry* **1975**, *14*, 5355–5373.

(2) Frauenfelder, H.; Sligar, S. G.; Wolynes, P. G. *Science* **1991**, *254*, 1598−1603.
(3) Xie, X. S. *J. Chem. Phys.* **2002**, *117*, 11024−11032.
(4) English, B. P.; Min, W.; van Oijen, A. M.; Lee, K. T.; Luo, G.; Sun, H.; Cherayil, B. J.; Kou, S. C.; Xie, X. S. *Nat. Chem. Biol.* **2006**, *2*, 87−94.
(5) Karplus, M. *J. Phys. Chem. B* **2000**, *104*, 11−27.
(6) Boehr, D. D.; Nussinov, R.; Wright, P. E. *Nat. Chem. Biol.* **2009**, *5*, 789−796.
(7) Clore, G. M.; Iwahara, J. *Chem. Rev.* **2009**, *109*, 4108−4139.
(8) Sugase, K.; Dyson, H. J.; Wright, P. E. *Nature* **2007**, *447*, 1021−1025.
(9) Fraser, J. S.; Clarkson, M. W.; Degnan, S. C.; Erion, R.; Kern, D.; Alber, T. *Nature* **2009**, *462*, 669−673.
(10) Bouvignies, G.; Vallurupalli, P.; Hansen, D. F.; Correia, B. E.; Lange, O.; Bah, A.; Vernon, R. M.; Dahlquist, F. W.; Baker, D.; Kay, L. E. *Nature* **2011**, *477*, 111−114.
(11) Korzhnev, D. M.; Religa, T. L.; Banachewicz, W.; Fersht, A. R.; Kay, L. E. *Science* **2010**, *329*, 1312−1316.
(12) Bouvignies, G.; Hansen, D. F.; Vallurupalli, P.; Kay, L. E. *J. Am. Chem. Soc.* **2011**, *133*, 1935−1945.
(13) Palmer, A. G., III; Kroenke, C. D.; Loria, J. P. *Methods Enzymol.* **2001**, *339*, 204−238.
(14) Palmer, A. G., III. *Chem. Rev.* **2004**, *104*, 3623−3640.
(15) Mittermaier, A.; Kay, L. E. *Science* **2006**, *312*, 224−228.
(16) Meiboom, S.; Gill, D. *Rev. Sci. Instrum.* **1958**, *29*, 688−691.
(17) Carr, H. Y.; Purcell, E. M. *Phys. Rev.* **1954**, *94*, 630−638.
(18) Korzhnev, D. M.; Salvatella, X.; Vendruscolo, M.; Di Nardo, A. A.; Davidson, A. R.; Dobson, C. M.; Kay, L. E. *Nature* **2004**, *430*, 586−590.
(19) Hansen, D. F.; Vallurupalli, P.; Lundstrom, P.; Neudecker, P.; Kay, L. E. *J. Am. Chem. Soc.* **2008**, *130*, 2667−2675.
(20) Ishima, R.; Wingfield, P. T.; Stahl, S. J.; Kaufman, J. D.; Torchia, D. A. *J. Am. Chem. Soc.* **1998**, *120*, 10534−10542.
(21) Loria, J. P.; Rance, M.; Palmer, A. G., III. *J. Am. Chem. Soc.* **1999**, *121*, 2331−2332.
(22) Lundstrom, P.; Hansen, D. F.; Kay, L. E. *J. Biomol. NMR* **2008**, *42*, 35−47.
(23) Lundstrom, P.; Hansen, D. F.; Vallurupalli, P.; Kay, L. E. *J. Am. Chem. Soc.* **2009**, *131*, 1915−1926.
(24) Lundstrom, P.; Lin, H.; Kay, L. E. *J. Biomol. NMR* **2009**, *44*, 139−155.
(25) Hansen, A. L.; Kay, L. E. *J. Biomol. NMR* **2011**, *50*, 347−355.
(26) Mulder, F. A.; Skrynnikov, N. R.; Hon, B.; Dahlquist, F. W.; Kay, L. E. *J. Am. Chem. Soc.* **2001**, *123*, 967−975.
(27) Skrynnikov, N. R.; Mulder, F. A.; Hon, B.; Dahlquist, F. W.; Kay, L. E. *J. Am. Chem. Soc.* **2001**, *123*, 4556−4566.
(28) Vallurupalli, P.; Hansen, D. F.; Stollar, E.; Meirovitch, E.; Kay, L. E. *Proc. Natl. Acad. Sci. U.S.A.* **2007**, *104*, 18473−18477.
(29) Hansen, D. F.; Vallurupalli, P.; Kay, L. E. *J. Am. Chem. Soc.* **2008**, *130*, 8397−8405.
(30) Vallurupalli, P.; Hansen, D. F.; Kay, L. E. *Proc. Natl. Acad. Sci. U.S.A.* **2008**, *105*, 11766−11771.
(31) Vallurupalli, P.; Bouvignies, G.; Kay, L. E. *J. Phys. Chem. B* **2011**, *115*, 14891−14900.
(32) Farrow, N. A.; Zhang, O.; Forman-Kay, J. D.; Kay, L. E. *J. Biomol. NMR* **1994**, *4*, 727−734.
(33) Neudecker, P.; Lundstrom, P.; Kay, L. E. *Biophys. J.* **2009**, *96*, 2045−2054.
(34) Forsén, S.; Hoffman, R. A. *J. Chem. Phys.* **1963**, *39*, 2892−2901.
(35) Fawzi, N. L.; Ying, J.; Ghirlando, R.; Torchia, D. A.; Clore, G. M. *Nature* **2011**, *480*, 268−72.
(36) Bertini, I.; Ciurli, S.; Dikiy, A.; Gasanov, R.; Luchinat, C.; Martini, G.; Safarov, N. *J. Am. Chem. Soc.* **1999**, *121*, 2037−2046.
(37) Ward, K. M.; Aletras, A. H.; Balaban, R. S. *J. Magn. Reson.* **2000**, *143*, 79−87.
(38) Zhou, J. Y.; van Zijl, P. C. M. *Prog. Nucl. Magn. Reson. Spectrosc.* **2006**, *48*, 109−136.
(39) Hansen, D. F.; Led, J. J. *Proc. Natl. Acad. Sci. U.S.A.* **2006**, *103*, 1738−1743.
(40) Gupta, R. K.; Redfield, A. G. *Science* **1970**, *169*, 1204−1206.
(41) Cayley, P. J.; Albrand, J. P.; Feeney, J.; Roberts, G. C.; Piper, E. A.; Burgen, A. S. *Biochemistry* **1979**, *18*, 3886−3895.
(42) van Zijl, P. C. M.; Yadav, N. N. *Magn. Reson. Med.* **2011**, *65*, 927−948.
(43) Jemth, P.; Day, R.; Gianni, S.; Khan, F.; Allen, M.; Daggett, V.; Fersht, A. R. *J. Mol. Biol.* **2005**, *350*, 363−378.
(44) Loria, J. P.; Rance, M.; Palmer, A. G., III. *J. Biomol. NMR* **1999**, *15*, 151−155.
(45) Palmer, A. G., III; Grey, M. J.; Wang, C. *Methods Enzymol.* **2005**, *394*, 430−465.
(46) Korzhnev, D. M.; Kloiber, K.; Kanelis, V.; Tugarinov, V.; Kay, L. E. *J. Am. Chem. Soc.* **2004**, *126*, 3964−3973.
(47) Millet, O.; Loria, J. P.; Kroenke, C. D.; Pons, M.; Palmer, A. G. *J. Am. Chem. Soc.* **2000**, *122*, 2867−2877.
(48) Zhou, J. Y.; Wilson, D. A.; Sun, P. Z.; Klaus, J. A.; van Zijl, P. C. M. *Magn. Reson. Med.* **2004**, *51*, 945−952.
(49) Roell, S. A.; Dreher, W.; Leibfritz, D. *J. Magn. Reson.* **1998**, *132*, 96−101.
(50) Farrow, N. A.; Muhandiram, R.; Singer, A. U.; Pascal, S. M.; Kay, C. M.; Gish, G.; Shoelson, S. E.; Pawson, T.; Forman-Kay, J. D.; Kay, L. E. *Biochemistry* **1994**, *33*, 5984−6003.
(51) Morris, G. A.; Freeman, R. *J. Am. Chem. Soc.* **1979**, *101*, 760−762.
(52) Pervushin, K.; Riek, R.; Wider, G.; Wuthrich, K. *Proc. Natl. Acad. Sci. U.S.A.* **1997**, *94*, 12366−12371.
(53) Goldman, M. *J. Magn. Reson.* **1984**, *60*, 437−452.
(54) Levitt, M. H. *J. Magn. Reson.* **1982**, *50*, 95−110.
(55) Rance, M.; Loria, J. P.; Palmer, A. G., III. *J. Magn. Reson.* **1999**, *136*, 92−101.
(56) Kay, L. E.; Keifer, P.; Saarinen, T. *J. Am. Chem. Soc.* **1992**, *114*, 10663−10665.
(57) Schleucher, J.; Sattler, M.; Griesinger, C. *Angew. Chem., Int. Ed. Engl.* **1993**, *32*, 1489−1491.
(58) Marion, D.; Ikura, M.; Tschudin, R.; Bax, A. *J. Magn. Reson.* **1989**, *85*, 393−399.
(59) Shaka, A. J.; Keeler, J.; Frenkiel, T.; Freeman, R. *J. Magn. Reson.* **1983**, *52*, 335−338.
(60) Korzhnev, D. M.; Vernon, R. M.; Religa, T. L.; Hansen, A. L.; Baker, D.; Fersht, A. R.; Kay, L. E. *J. Am. Chem. Soc.* **2011**, *133*, 10974−10982.
(61) Grey, M. J.; Tang, Y.; Alexov, E.; McKnight, C. J.; Raleigh, D. P.; Palmer, A. G., III. *J. Mol. Biol.* **2006**, *355*, 1078−1094.
(62) Jemth, P.; Gianni, S.; Day, R.; Li, B.; Johnson, C. M.; Daggett, V.; Fersht, A. R. *Proc. Natl. Acad. Sci. U.S.A.* **2004**, *101*, 6450−6455.
(63) Clore, G. M.; Roberts, G. C. K.; Gronenborn, A.; Birdsall, B.; Feeney, J. *J. Magn. Reson.* **1981**, *45*, 151−161.
(64) Tamiola, K.; Acar, B.; Mulder, F. A. *J. Am. Chem. Soc.* **2010**, *132*, 18000−18003.
(65) Farrow, N. A.; Zhang, O.; Forman-Kay, J. D.; Kay, L. E. *Biochemistry* **1995**, *34*, 868−878.
(66) Palmer, A. G., III; Massi, F. *Chem. Rev.* **2006**, *106*, 1700−1719.
(67) Wagner, G.; DeMarco, A.; Wuthrich, K. *Biophys. Struct. Mech.* **1976**, *2*, 139−158.
(68) Montelione, G. T.; Wagner, G. *J. Am. Chem. Soc.* **1989**, *111*, 3096−3098.
(69) Clore, G. M.; Driscoll, P. C.; Wingfield, P. T.; Gronenborn, A. M. *Biochemistry* **1990**, *29*, 7387−7401.
(70) Clore, G. M.; Omichinski, J. G.; Gronenborn, A. M. *J. Am. Chem. Soc.* **1991**, *113*, 4350−4351.
(71) Mittermaier, A.; Kay, L. E. *J. Am. Chem. Soc.* **2001**, *123*, 6892−6903.
(72) Guenneugues, M.; Berthault, P.; Desvaux, H. *J. Magn. Reson.* **1999**, *136*, 118−126.
(73) Hansen, D. F.; Vallurupalli, P.; Kay, L. E. *J. Phys. Chem. B* **2008**, *112*, 5898−5904.

(74) Delaglio, F.; Grzesiek, S.; Vuister, G. W.; Zhu, G.; Pfeifer, J.; Bax, A. *J. Biomol. NMR* **1995**, *6*, 277−293.
(75) Available at http://pound.med.utoronto.ca/software.html.
(76) Goddard, T. D.; Kneller, D. G. *SPARKY 3* University of California: San Francisco, 2008.
(77) McConnell, H. M. *J. Chem. Phys.* **1958**, *28*, 430−431.